

# Honeycomb AgSe Monolayer Nanosheets for Studying Two-dimensional Dirac Nodal Line Fermions

Jianchen Lu, Lei Gao, Shiru Song, Hang Li, Gefei Niu, Hui Chen, Tian Qian, Hong Ding, Xiao Lin,\* Shixuan Du,\* and Hong-Jun Gao



Cite This: *ACS Appl. Nano Mater.* 2021, 4, 8845–8850



Read Online

ACCESS |



Metrics & More



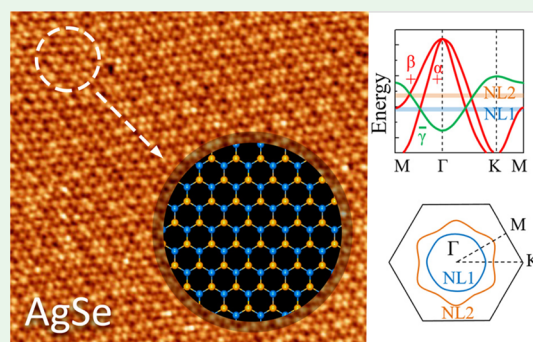
Article Recommendations



Supporting Information

**ABSTRACT:** Two-dimensional (2D) materials are interesting for both fundamental properties and potential applications. Among them, the recently fabricated transition-metal monochalcogenides (TMMs) possess Dirac nodal line fermions and can serve as a model to explore topologically nontrivial quantum spin Hall edge states. Here, we successfully fabricated a flat AgSe monolayer nanosheet via direct selenization of a Ag(111) substrate at room temperature. The AgSe monolayer is characterized at the atomic scale by high-resolution scanning tunneling microscopy combined with low-energy electron diffraction, angle-resolved photoemission spectroscopy, and density functional theory (DFT) calculations. The results show that the AgSe monolayer endowed with a honeycomb lattice grows incommensurately on the Ag(111) substrate and exhibits a semiconductor behavior. In addition, DFT calculations reveal that the free-standing AgSe monolayer possesses two 2D Dirac nodal line fermions protected by mirror reflection symmetry without considering the spin–orbit coupling. The realization and investigation of the flat honeycomb AgSe monolayer extend the scope of 2D TMMs and provide an opportunity to study 2D Dirac nodal line fermions.

**KEYWORDS:** transition-metal monochalcogenides, AgSe monolayer, scanning tunneling microscopy, 2D Dirac nodal line fermion, angle-resolved photoemission spectroscopy



## INTRODUCTION

Inspired by the great success of graphene in the past few decades, worldwide scientific efforts have been focused on exploring two-dimensional (2D) materials beyond graphene, driven by their potential applications in electronics and optoelectronics.<sup>1–3</sup> To date, a series of 2D materials has been successfully fabricated, for instance, monoatomic 2D materials (silicene,<sup>4</sup> germanene,<sup>5</sup> borophene,<sup>6</sup> stanene,<sup>7</sup> and antimonene<sup>8</sup>) and binary 2D materials (hexagonal boron nitride,<sup>9</sup> transition-metal dichalcogenides,<sup>10</sup> and transition-metal monochalcogenides (TMMs)<sup>11–15</sup>). Among them, 2D TMMs have drawn a high level of attention in recent years. The investigations of 2D TMM materials have not only enriched the 2D material library but also offered some novel physical properties<sup>11–14,16</sup> and potential applications in high-speed low-dissipation devices.<sup>17,18</sup> Previously, we reported the successful fabrication of a CuSe honeycomb monolayer on a Cu(111) substrate, which exhibits a Dirac nodal line fermion (DNLF) feature, protected by mirror reflection symmetry.<sup>13</sup> Recently, Liu et al. have realized a flat AgTe monolayer with a honeycomb structure on a Ag(111) substrate, which also possesses the DNLF electronic properties.<sup>12</sup>

Silver selenides, one of the transition-metal chalcogenides, exhibit interesting structural, optical, and electrical proper-

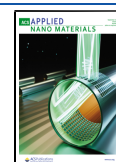
ties.<sup>19,20</sup> Ag<sub>2</sub>Se, the only stable composition of bulk silver selenides, is a promising candidate for thermoelectric materials, especially near room temperature.<sup>21</sup> In addition, single-crystalline  $\beta$ -Ag<sub>2</sub>Se nanostructures are confirmed to be a new class of three-dimensional topological insulators,<sup>22</sup> and Ag<sub>2</sub>Se quantum dots are demonstrated to have potential applications in bioimaging.<sup>23</sup> Moreover, nonstoichiometric silver selenide (Ag<sub>2+ $\delta$</sub> Se) exhibits an unusually high magnetoresistance in spite of the nonmagnetic nature in Ag<sub>2+ $\delta$</sub> Se.<sup>24</sup> Although silver selenide films have been fabricated,<sup>20,25</sup> it is still a great challenge to obtain silver selenide monolayers with different stoichiometric ratios.

Here, we report epitaxy growth and characterization of a silver selenide (AgSe) monolayer nanosheet by direct selenization of the Ag(111) substrate. Our results show that the AgSe monolayer adopts a planar structure and possesses a honeycomb lattice with alternative arrangements of silver and

Received: June 9, 2021

Accepted: August 18, 2021

Published: August 27, 2021



selenium atoms, confirmed by the combination of scanning tunneling microscopy (STM), low-energy electron diffraction (LEED), and density functional theory (DFT). The band structure of the AgSe monolayer on Ag(111) is revealed by angle-resolved photoemission spectroscopy (ARPES) and scanning tunneling spectroscopy (STS), showing the semi-conducting feature of the AgSe monolayer on Ag(111). Importantly, DFT calculations reveal that the free-standing AgSe monolayer is endowed with DNLFs, protected by mirror reflection symmetry when spin-orbit coupling (SOC) is ignored. Furthermore, DFT calculations demonstrate that the AgSe monolayer on an inert substrate like graphene could be a candidate for a 2D material with DNLFs.

## RESULTS AND DISCUSSION

The AgSe monolayer was grown by direct one-step selenization of a Ag(111) substrate (see the schematic diagram shown in Figure 1a). Selenium atoms were deposited directly

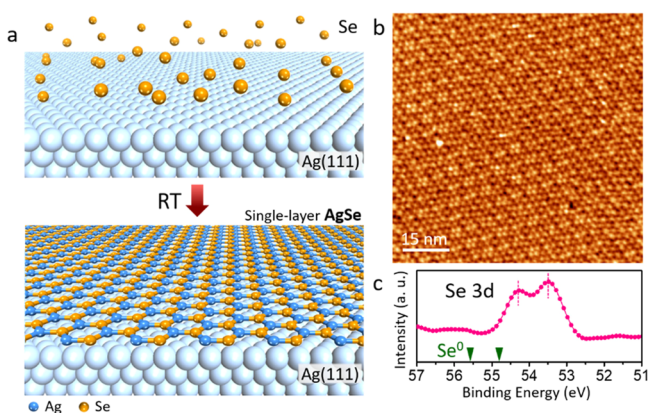


**Figure 1.** Growth process and STM and XPS characterizations of the AgSe monolayer on the Ag(111) substrate. (a) Schematic diagram of the fabrication process. The Ag spheres with different sizes and colors are applied to distinguish the Ag atoms in the Ag(111) substrate and the AgSe monolayer. (b) Large-scale STM image ( $U = -0.5$  V and  $I = 0.8$  nA) showing the homogenous and uniform AgSe monolayer with clearly distinct moiré patterns on Ag(111). (c) XPS measurements for the binding energies of Se 3d. Two green triangles indicate the peak positions (55.68 and 54.80 eV) corresponding to the binding energy of pure selenium.

onto the clean Ag(111) substrate, while the substrate was kept at room temperature during the deposition. The growth of the AgSe monolayer was finished fully at room temperature. The chemical structure of the AgSe monolayer is similar to a boron nitride monolayer with an alternative arrangement of Se elements and Ag elements in a honeycomb six-membered ring. To investigate the atomic arrangement of the sample surface, we characterized it by STM. Figure 1b shows a large-scale STM image of the as-grown sample. The STM image shows well-ordered moiré patterns, which can be more clearly identified in a zoomed-in STM image shown in Figure S1a. The periodicity of the moiré patterns is  $\sim 25.4$  Å according to the line profile shown in Figure S1b. In addition, X-ray photoemission spectroscopy (XPS) was used to identify the chemical states of Se in the sample surface. Figure 1c shows the Se 3d core-level XPS spectrum for the AgSe sample. There are two typical peaks at binding energies of 54.27 and 53.47 eV (labeled by the red dashed lines) for Se  $3d_{3/2}$  and  $3d_{5/2}$ , respectively. To emphasize the oxidation state of selenium, we

mark the binding energy positions for pure selenium in Figure 1c (two green triangles).<sup>26</sup> It can be seen that the Se element in the AgSe monolayer is not in its zero state but close to a  $-2$  chemical state,<sup>27</sup> indicating that chemical bonds exist between Se and Ag atoms at the epitaxial interface. It should be noted that the XPS data shown in Figure 1c show no silver surface states, which may indicate the strong coupling between the AgSe monolayer and the Ag(111) substrate. Additionally, we also measured the binding energies of Ag  $3d_{3/2}$  and Ag  $3d_{5/2}$  in our sample, as shown in Figure S2. Due to the fact that XPS collects photoelectron signals from several nanometers under the sample surface, the detected Ag  $3d_{3/2}$  (374.2 eV) and Ag  $3d_{5/2}$  (368.2 eV) signals were mainly dominated by the Ag(111) substrate.

To obtain the structural information and epitaxial relation on the as-grown sample, we carried out a 2D fast Fourier transform (2D-FFT) analysis on STM images and LEED measurements. Figure S3b shows a 2D-FFT image obtained on an atomic-resolution STM image of the AgSe monolayer shown in Figure S3a. The green and yellow arrows label spots from the superstructure (moiré pattern) and the AgSe lattice, respectively. As shown in the 2D-FFT image, the moiré pattern spots are slightly rotated with regard to the AgSe spots at an angle of  $\theta = 16 \pm 0.3^\circ$ . The angle and the moiré periodicity are representative of all AgSe monolayers observed in our experiment, indicating that a fixed epitaxial relationship is present for the whole AgSe/Ag(111) sample. In addition, a typical LEED pattern was also obtained for the 10 mm-diameter AgSe/Ag(111) sample, as shown in Figure 2a. The outmost six diffraction spots (marked by the white circles) are assigned to the sixfold symmetry of the Ag(111) substrate, and the diffraction spots (marked by two yellow circles) are related to the AgSe lattice. The other diffraction spots result from the moiré patterns. Figure S4b shows a zoomed-in LEED pattern of AgSe/Ag(111) at 30 eV, demonstrating clearly three pairs of diffraction spots in which the top two correspond to spots from the AgSe lattice and the other one comes from the moiré patterns.

In order to characterize the AgSe monolayer in detail, we subsequently carried out STM measurements. Figure 2b shows a high-resolution STM image of the AgSe monolayer, which exhibits hexagonal close-packed protrusions with a unit cell of  $a = 0.5 \pm 0.05$  nm,  $b = 0.5 \pm 0.05$  nm, and  $\alpha = 60^\circ$  marked by a red rhombus. A moiré pattern marked by a black rhombus is also observed in Figure 2b. To obtain a detailed structural analysis of the AgSe monolayer on the Ag(111) substrate, we carried out DFT calculations. Figure 2c shows the optimized configuration of AgSe/Ag(111). The upper panel clearly shows that the AgSe monolayer adopts a honeycomb lattice with alternating Se atoms and Ag atoms. The distance between two nearest Se atoms is measured to be 5.0 Å, which is close to the distance between two protrusions shown in Figure 2b. The angle between the moiré superstructure marked by a black rhombus and the AgSe lattice in Figure 2c is about  $16^\circ$ , which agrees well with the experimental results shown in Figure S3b. In addition, a flat structure of the AgSe monolayer is identified from the side view (lower panel of Figure 2c). Figure 2d shows the corresponding simulated STM image based on the optimized configuration shown in Figure 2c. The overall features of the experimental STM image (Figure 2b) are well produced. The remarkable agreement between the STM simulation and the experimental STM observation strongly

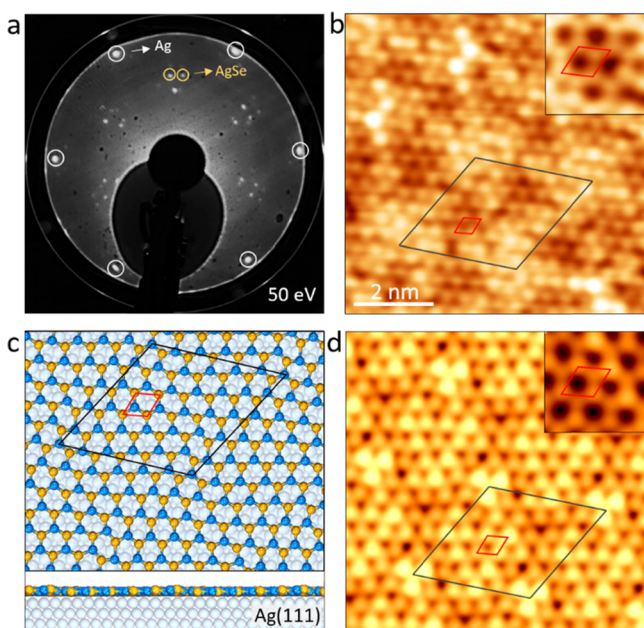


**Figure 2.** LEED pattern and atomic configurations of the AgSe monolayer on the Ag(111) substrate. (a) LEED pattern of the AgSe monolayer on Ag(111). The white and yellow circles indicate the diffraction spots from the Ag(111) lattice and the AgSe monolayer, respectively. The other spots correspond to the moiré patterns. (b) Highly resolved STM image of the AgSe monolayer ( $U = -0.1$  V and  $I = 0.4$  nA). The black and red rhombuses represent the unit cells of the AgSe monolayer and moiré patterns, respectively. The inset in the top-right corner shows an ultrahighly resolved STM image of the AgSe monolayer ( $1.6$  nm  $\times$   $1.6$  nm,  $U = -0.01$  V, and  $I = 30$  nA) obtained by a special tip state. (c) DFT-optimized atomic configuration of the AgSe monolayer on the Ag(111) substrate in top and side views, demonstrating a graphene-like honeycomb lattice. (d) Simulated STM image. The top-right corner shows a simulated STM image with a honeycomb lattice.

demonstrates the successful growth of a large-scale, high-quality AgSe monolayer on the Ag(111) substrate.

The typical STM image of the AgSe monolayer shown in Figure 2b shows that only hexagonally arranged Se atoms are imaged, confirmed by the simulated STM image shown in Figure 2d. Interestingly, a honeycomb structure of the AgSe monolayer was also obtained by a special tip state during the STM scanning (top-right in Figure 2b) in which a six-membered ring structure was clearly identified. Importantly, the honeycomb structure is reproduced in the simulated STM image of the AgSe monolayer (top-right in Figure 2d). However, in most STM images, the AgSe monolayer exhibits a hexagonal lattice because of the larger size and the higher number of electronic states of the Se atom compared to the Ag atom, similar to other 2D TMM materials.<sup>12–14</sup>

By considering the optimized atomic configuration of the AgSe/Ag(111) system shown in Figure 2c, we conclude that the well-defined moiré patterns of the AgSe monolayer on Ag(111) are described in the form of a matrix as

$$\text{moiré pattern} = \begin{pmatrix} 7 & 3 \\ -3 & 10 \end{pmatrix} \text{Ag(111)}$$

and the Se lattice of the AgSe monolayer on Ag(111) is described by the matrix

$$\text{AgSe} = \begin{pmatrix} 1.0322 & 0.8069 \\ -0.8066 & 1.8381 \end{pmatrix} \text{Ag(111)}$$

From the matrix, we found that the AgSe monolayer grows incommensurately on the Ag(111) substrate. Based on the above matrices, we simulated the LEED patterns of the AgSe monolayer with respect to the Ag(111) substrate and moiré patterns with respect to the Ag(111) substrate (Figure S4c,d), which show a good agreement with Figure S4a,b, indicating the formation of a large-scale and uniform AgSe monolayer on the Ag(111) substrate.

The AgSe monolayer sample is stable under ambient conditions at room temperature. To demonstrate this property, the sample was removed from the high-vacuum chamber and was kept in air without protection for more than 12 h. Then the sample was put back to the high-vacuum chamber and annealed at  $400$  °C for 12 h to remove possible adsorbates. LEED characterizations show that the sample kept its original pattern (see Figure S5 for details). The stability of the AgSe monolayer in air makes it suitable for potential applications under ambient conditions.

To study the electronic properties of the AgSe monolayer, we performed ARPES measurements. The samples were transferred from the MBE chamber to the ARPES facility without breaking the vacuum using a high-vacuum suitcase. Previous studies of 2D TMMs show that the strong intensity bands of the substrate usually are below  $-2$  eV.<sup>12,13</sup> We therefore measured the band dispersions of the AgSe monolayer on the Ag(111) substrate from 0 to  $-1.8$  eV along the  $M-\Gamma-K$  direction (Figure 3a). Same as for the

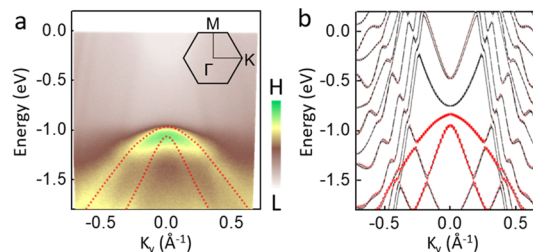


**Figure 3.** ARPES characterization and the DFT-calculated band structure of the AgSe monolayer on the Ag(111) substrate. (a) ARPES intensity plot measured along the  $M-\Gamma-K$  direction in the hexagonal Brillouin zone (inset). The red lines denote the bands of the AgSe monolayer. (b) Calculated band structure of the AgSe monolayer on a 10-layer Ag(111) substrate with considering SOC. The projected bands of the AgSe monolayer are marked by red lines.

AgTe monolayer on the Ag(111) substrate,<sup>12</sup> the surface states of Ag(111) were modulated by the epitaxy of the AgSe monolayer. Near the Fermi level, instead of electron-like bands of the Ag(111) substrate, two hole-like bands of the AgSe monolayer marked by red dashed lines were clearly observed, indicating the semiconducting nature of the AgSe monolayer. To understand the ARPES data, we calculated the projected band structures of the AgSe monolayer on a 10-layer Ag(111) substrate with considering SOC. A  $(1 \times 1)$  AgSe monolayer on a  $(\sqrt{3} \times \sqrt{3})$  Ag(111) substrate was used to reduce the huge computational capacity when using the supercell observed in STM experiments (Figure 2b). As shown in Figure 3b, the bands mainly contributed by the AgSe monolayer are denoted by red circles, which well reproduce the ARPES data. In addition, we also recorded the  $dI/dV$  spectrum of the AgSe

monolayer, as shown in Figure S6. The results show that the AgSe monolayer on the Ag(111) substrate has a band gap of 2.28 eV with a valence band maximum at  $-1.73$  eV and a conduction band minimum at  $0.55$  eV, where the valence band maximum position is in good agreement with the ARPES data shown in Figure 3a. The consistency of the ARPES data, STS curve, and DFT calculations further confirms unambiguously the successful fabrication of the flat AgSe monolayer on the Ag(111) substrate.

To further study the intrinsic electronic properties of the AgSe monolayer, a free-standing AgSe monolayer model is used to avoid the influence of the Ag(111) substrate. Figure 4a

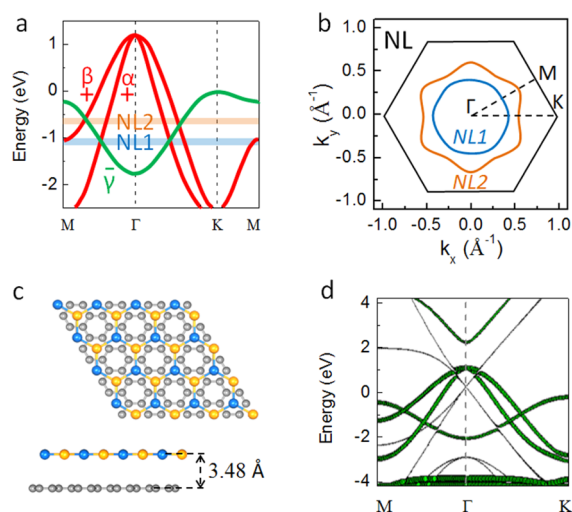


**Figure 4.** Calculated electronic structures of the free-standing AgSe monolayer and the AgSe monolayer on graphene. (a) Calculated band structure of the AgSe monolayer without considering the SOC effect. (b) Momentum distribution of two nodal line rings (NL1 and NL2). (c) Top and side views of the optimized atomic structure of the AgSe monolayer on a graphene substrate. (d) Calculated band structure of the AgSe monolayer on graphene without considering the SOC effect.

shows the calculated band structure for the free-standing AgSe monolayer without SOC. Near the Fermi level, there are three bands marked by  $\alpha$ ,  $\beta$ , and  $\gamma$ . Similar to other 2D TMMs CuSe and AgTe,<sup>12,13</sup> these bands can be divided into two groups,  $\alpha/\beta$  bands and  $\gamma$  band, according to the projected band structures (refer Figure S7 for more details). The  $\alpha/\beta$  bands are dominated by in-plane orbitals (Se  $p_x/p_y$  and Ag  $d_{xy}/d_{x^2-y^2}$ ), while the  $\gamma$  band is dominated by out-of-plane orbitals (Se  $p_z$  and Ag  $d_{xz}/d_{yz}$ ), respectively. It is worth noting that at the touching points, the  $\gamma$  band crosses both  $\alpha$  and  $\beta$  bands linearly without opening energy gaps, as denoted by orange and blue shaded regions in Figure 4a, forming two DNLFs (Figure 4b).

In order to further study the symmetry-protected characteristic of the two DNLF rings (NL1 and NL2), we analyze the irreducible representations (IRs) and the little groups for the three bands along the  $\Gamma$ -M and  $\Gamma$ -K directions. The IRs along the  $\Gamma$ -M direction for  $\alpha$ ,  $\beta$ , and  $\gamma$  bands are  $A_1$ ,  $B_1$ , and  $B_2$ , respectively, while those along the  $\Gamma$ -K direction are  $A'$ ,  $A'$ , and  $A''$ , respectively. The little group along the  $\Gamma$ -M direction is  $C_{2v}$  with mirror reflection symmetries  $M_{yz}$  and  $M_{xy}$ , while that along the  $\Gamma$ -K direction is  $C_s$  with the mirror reflection symmetry  $M_{xy}$ . Under the condition of  $M_{xy}$ , the IRs  $A''$  and  $B_2$  are odd,  $A'$ , while  $A_1$  and  $B_1$  are even. Therefore, the mirror parities for the  $\gamma$  and  $\alpha/\beta$  bands are odd and even, which are

denoted by “ $-$ ” and “ $+$ ”, respectively, in Figure 4a. The opposite mirror parities of these bands ensure the emergence of these two DNLs as shown in Figure 4b. When SOC is considered, the Dirac nodal lines are opened local gaps as shown in Figure S8. Similar to CuSe, the topological state changes to a topological insulating state.

When the AgSe monolayer is grown on the Ag(111) substrate, the  $\gamma$  band is annihilated due to the strong coupling between Ag(111) and the out-of-plane orbitals of AgSe, as was the case with the previously reported AgTe monolayer and CuSe monolayer.<sup>12,13</sup> Hence, the two DNLs were not observed in the ARPES experiment on AgSe/Ag(111) (Figure 3a). We then study the projected band structure of the AgSe monolayer on graphene in which the interlayer separation is  $3.48$  Å with weak coupling, as shown in Figure 4c. The two DNLs remain as shown in Figure 4d. Therefore, the AgSe monolayer fabricated on a weakly coupled substrate, such as graphene, is a promising candidate for producing intriguing 2D DNLFs.

## CONCLUSIONS

We have successfully fabricated a large-scale and high-quality honeycomb AgSe monolayer with alternative arrangements of Ag and Se atoms on the Ag(111) substrate, investigated by STM, LEED, XPS, ARPES, STS, and DFT. We found that the free-standing AgSe possesses two DNLFs protected by mirror reflection symmetry. However, we do not observe the DNLFs in the AgSe/Ag(111) sample due to the strong coupling between the AgSe monolayer and the Ag(111) substrate, and we theoretically predicted that the intriguing 2D DNLFs can be directly observed using ARPES if the AgSe monolayer can be synthesized on a weakly interacting substrate such as graphene.

## ASSOCIATED CONTENT

### Supporting Information

The Supporting Information is available free of charge at <https://pubs.acs.org/doi/10.1021/acsnm.1c01517>.

Sample preparation, characterization and DFT calculation details for the AgSe monolayer on the Ag(111) substrate, zoomed-in STM image and line profile, additional Ag 3d XPS spectrum of the AgSe monolayer on the Ag(111) substrate, FFT image of the AgSe monolayer, additional experimental and simulated LEED patterns, LEED patterns of the AgSe sample after exposure to air,  $dI/dV$  spectrum of the AgSe monolayer on the Ag(111) substrate, calculated orbital projected band structures of the AgSe monolayer, and calculated band structure of the AgSe monolayer with SOC (PDF)

## AUTHOR INFORMATION

### Corresponding Authors

Xiao Lin – Institute of Physics & University of Chinese Academy of Sciences and CAS Center for Excellence in Topological Quantum Computation, Chinese Academy of Sciences, Beijing 100190, P. R. China; [orcid.org/0000-0002-2490-4691](https://orcid.org/0000-0002-2490-4691); Email: [xlin@ucas.ac.cn](mailto:xlin@ucas.ac.cn)

Shixuan Du – Institute of Physics & University of Chinese Academy of Sciences and CAS Center for Excellence in Topological Quantum Computation, Chinese Academy of Sciences, Beijing 100190, P. R. China; [orcid.org/0000-0001-9323-1307](https://orcid.org/0000-0001-9323-1307); Email: [sxdu@iphy.ac.cn](mailto:sxdu@iphy.ac.cn)

## Authors

**Jianchen Lu** – Institute of Physics & University of Chinese Academy of Sciences, Chinese Academy of Sciences, Beijing 100190, P. R. China; Faculty of Materials Science and Engineering, Kunming University of Science and Technology, Kunming, Yunnan 650093, P. R. China; [orcid.org/0000-0002-2120-4948](https://orcid.org/0000-0002-2120-4948)

**Lei Gao** – Institute of Physics & University of Chinese Academy of Sciences, Chinese Academy of Sciences, Beijing 100190, P. R. China; Faculty of Science, Kunming University of Science and Technology, Kunming, Yunnan 650093, P. R. China; [orcid.org/0000-0002-9018-3167](https://orcid.org/0000-0002-9018-3167)

**Shiru Song** – Institute of Physics & University of Chinese Academy of Sciences, Chinese Academy of Sciences, Beijing 100190, P. R. China; Faculty of Materials Science and Engineering, Kunming University of Science and Technology, Kunming, Yunnan 650093, P. R. China

**Hang Li** – Institute of Physics & University of Chinese Academy of Sciences, Chinese Academy of Sciences, Beijing 100190, P. R. China

**Gefei Niu** – Faculty of Materials Science and Engineering, Kunming University of Science and Technology, Kunming, Yunnan 650093, P. R. China

**Hui Chen** – Institute of Physics & University of Chinese Academy of Sciences, Chinese Academy of Sciences, Beijing 100190, P. R. China

**Tian Qian** – Institute of Physics & University of Chinese Academy of Sciences, Chinese Academy of Sciences, Beijing 100190, P. R. China

**Hong Ding** – Institute of Physics & University of Chinese Academy of Sciences and CAS Center for Excellence in Topological Quantum Computation, Chinese Academy of Sciences, Beijing 100190, P. R. China

**Hong-Jun Gao** – Institute of Physics & University of Chinese Academy of Sciences and CAS Center for Excellence in Topological Quantum Computation, Chinese Academy of Sciences, Beijing 100190, P. R. China; [orcid.org/0000-0002-6766-0623](https://orcid.org/0000-0002-6766-0623)

Complete contact information is available at: <https://pubs.acs.org/10.1021/acsnm.1c01517>

## Author Contributions

H.-J.G., S.X.D., and X.L. conceived and coordinated the research project. J.C.L. and H.C. performed the growth and STM measurements. L.G. and S.R.S. carried out theoretical calculations. H.L. performed the APRES experiments under the guidance of T.Q. and H.D. J.C.L. and G.F.N. drafted and edited the manuscript. All authors participated in discussing the data. J.C.L., L.G., and S.R.S. contributed equally to this study.

## Notes

The authors declare no competing financial interest.

## ACKNOWLEDGMENTS

We thank Werner A. Hofer for helpful suggestions. This study was supported by the National Key Research and Development Projects of China (2018YFA0305800 and 2019YFA0308500), the National Natural Science Foundation of China (61901200 and 61925111), the Yunnan Fundamental Research Projects (2019FD041 and 202101AW070010), the Strategic Priority Research Program of Chinese Academy of Sciences (XDB30010000 and XDB28000000), the China Postdoctoral

Science Foundation, and the Yunnan Province Postdoctoral Science Foundation.

## REFERENCES

- (1) Novoselov, K. S.; Geim, A. K.; Morozov, S. V.; Jiang, D.; Katsnelson, M. I.; Grigorieva, I. V.; Dubonos, S. V.; Firsov, A. A. Two-dimensional gas of massless Dirac fermions in graphene. *Nature* **2005**, *438*, 197–200.
- (2) Wang, Q. H.; Kalantar-Zadeh, K.; Kis, A.; Coleman, J. N.; Strano, M. S. Electronics and optoelectronics of two-dimensional transition metal dichalcogenides. *Nat. Nanotechnol.* **2012**, *7*, 699–712.
- (3) Li, G.; Zhang, Y. Y.; Guo, H.; Huang, L.; Lu, H.; Lin, X.; Wang, Y. L.; Du, S.; Gao, H. J. Epitaxial growth and physical properties of 2D materials beyond graphene: from monatomic materials to binary compounds. *Chem. Soc. Rev.* **2018**, *47*, 6073–6100.
- (4) Meng, L.; Wang, Y.; Zhang, L.; du, S.; Wu, R.; Li, L.; Zhang, Y.; Li, G.; Zhou, H.; Hofer, W. A.; Gao, H. J. Buckled silicene formation on Ir(111). *Nano Lett.* **2013**, *13*, 685–690.
- (5) Li, L.; Lu, S.-Z.; Pan, J.; Qin, Z.; Wang, Y.-Q.; Wang, Y.; Cao, G.-Y.; Du, S.; Gao, H.-J. Buckled germanene formation on Pt(111). *Adv. Mater.* **2014**, *26*, 4820–4824.
- (6) Feng, B.; Zhang, J.; Zhong, Q.; Li, W.; Li, S.; Li, H.; Cheng, P.; Meng, S.; Chen, L.; Wu, K. Experimental realization of two-dimensional boron sheets. *Nat. Chem.* **2016**, *8*, 563–568.
- (7) Zhu, F. F.; Chen, W. J.; Xu, Y.; Gao, C. L.; Guan, D. D.; Liu, C. H.; Qian, D.; Zhang, S. C.; Jia, J. F. Epitaxial growth of two-dimensional stanene. *Nat. Mater.* **2015**, *14*, 1020–1025.
- (8) Shao, Y.; Liu, Z. L.; Cheng, C.; Wu, X.; Liu, H.; Liu, C.; Wang, J. O.; Zhu, S. Y.; Wang, Y. Q.; Shi, D. X.; Ibrahim, K.; Sun, J. T.; Wang, Y. L.; Gao, H. J. Epitaxial growth of flat antimonene monolayer: a new honeycomb analogue of graphene. *Nano Lett.* **2018**, *18*, 2133–2139.
- (9) Farwick zum Hagen, F. H.; Zimmermann, D. M.; Silva, C. C.; Schlueter, C.; Atodiresei, N.; Jolie, W.; Martínez-Galera, A. J.; Dombrowski, D.; Schröder, U. A.; Will, M.; Lazić, P.; Caciuc, V.; Blügel, S.; Lee, T.-L.; Michely, T.; Busse, C. Structure and growth of hexagonal boron nitride on Ir(111). *ACS Nano* **2016**, *10*, 11012–11026.
- (10) Lu, J.; Bao, D. L.; Qian, K.; Zhang, S.; Chen, H.; Lin, X.; Du, S. X.; Gao, H. J. Identifying and visualizing the edge terminations of single-layer MoSe<sub>2</sub> island epitaxially grown on Au(111). *ACS Nano* **2017**, *11*, 1689–1695.
- (11) Dong, L.; Wang, A.; Li, E.; Wang, Q.; Li, G.; Huan, Q.; Gao, H.-J. Formation of two-dimensional AgTe monolayer atomic crystal on a Ag(111) substrate. *Chin. Phys. Lett.* **2019**, *36*, No. 028102.
- (12) Liu, B.; Liu, J.; Miao, G.; Xue, S.; Zhang, S.; Liu, L.; Huang, X.; Zhu, X.; Meng, S.; Guo, J.; Liu, M.; Wang, W. Flat AgTe honeycomb monolayer on Ag(111). *J. Phys. Chem. Lett.* **2019**, *10*, 1866–1871.
- (13) Gao, L.; Sun, J. T.; Lu, J. C.; Li, H.; Qian, K.; Zhang, S.; Zhang, Y. Y.; Qian, T.; Ding, H.; Lin, X.; Du, S.; Gao, H. J. Epitaxial growth of honeycomb monolayer CuSe with Dirac nodal line fermions. *Adv. Mater.* **2018**, *30*, No. 1707055.
- (14) Lin, X.; Lu, J. C.; Shao, Y.; Zhang, Y. Y.; Wu, X.; Pan, J. B.; Gao, L.; Zhu, S. Y.; Qian, K.; Zhang, Y. F.; Bao, D. L.; Li, L. F.; Wang, Y. Q.; Liu, Z. L.; Sun, J. T.; Lei, T.; Liu, C.; Wang, J. O.; Ibrahim, K.; Leonard, D. N.; Zhou, W.; Guo, H. M.; Wang, Y. L.; Du, S. X.; Pantelides, S. T.; Gao, H. J. Intrinsically patterned two-dimensional materials for selective adsorption of molecules and nanoclusters. *Nat. Mater.* **2017**, *16*, 717–721.
- (15) Wang, X.; Ruan, Z.; Du, R.; Zhang, H.; Yang, X.; Niu, G.; Cai, J.; Lu, J. Structural characterizations and electronic properties of CuSe monolayer endowed with triangular nanopores. *J. Mater. Sci.* **2021**, *56*, 10406–10413.
- (16) Gao, L.; Sun, J. T.; Sethi, G.; Zhang, Y. Y.; du, S.; Liu, F. Orbital design of topological insulators from two-dimensional semiconductors. *Nanoscale* **2019**, *11*, 22743–22747.
- (17) Feng, B.; Fu, B.; Kasamatsu, S.; Ito, S.; Cheng, P.; Liu, C. C.; Feng, Y.; Wu, S.; Mahatha, S. K.; Sheverdyeva, P.; Moras, P.; Arita, M.; Sugino, O.; Chiang, T. C.; Shimada, K.; Miyamoto, K.; Okuda, T.; Wu, K.; Chen, L.; Yao, Y.; Matsuda, I. Experimental realization of

two-dimensional Dirac nodal line fermions in monolayer Cu<sub>2</sub>Si. *Nat. Commun.* **2017**, *8*, 1007.

(18) Cameau, M.; Yukawa, R.; Chen, C. H.; Huang, A.; Ito, S.; Ishibiki, R.; Horiba, K.; Obata, Y.; Kondo, T.; Kumigashira, H.; Jeng, H. T.; D'Angelo, M.; Matsuda, I. Electronic structure of a monoatomic Cu<sub>2</sub>Si layer on a Si(111) substrate. *Phys. Rev. Mater.* **2019**, *3*, No. 044004.

(19) Yang, D.; Benton, A.; He, J.; Tang, X. Novel synthesis recipes boosting thermoelectric study of A<sub>2</sub>Q (A = Cu, Ag; Q = S, Se, Te). *J. Phys. D: Appl. Phys.* **2020**, *53*, 193001.

(20) Gao, J.; Miao, L.; Lai, H.; Zhu, S.; Peng, Y.; Wang, X.; Koumoto, K.; Cai, H. Thermoelectric flexible silver selenide films: compositional and length optimization. *iScience* **2020**, *23*, No. 100753.

(21) Ferhat, M.; Nagao, J. Thermoelectric and transport properties of  $\beta$ -Ag<sub>2</sub>Se compounds. *J. Appl. Phys.* **2000**, *88*, 813–816.

(22) Kim, J.; Hwang, A.; Lee, S. H.; Jhi, S. H.; Lee, S.; Park, Y. C.; Kim, S. I.; Kim, H. S.; Doh, Y. J.; Kim, J.; Kim, B. Quantum Electronic Transport of Topological Surface States in  $\beta$ -Ag<sub>2</sub>Se Nanowire. *ACS Nano* **2016**, *10*, 3936–3943.

(23) Gu, Y. P.; Cui, R.; Zhang, Z. L.; Xie, Z. X.; Pang, D. W. Ultrasmall near-infrared Ag<sub>2</sub>Se quantum dots with tunable fluorescence for in vivo imaging. *J. Am. Chem. Soc.* **2012**, *134*, 79–82.

(24) Xu, R.; Husmann, A.; Rosenbaum, T. F.; Saboungi, M. L.; Enderby, J. E.; Littlewood, P. B. Large magnetoresistance in non-magnetic silver chalcogenides. *Nature* **1997**, *390*, 57–60.

(25) Ding, Y.; Qiu, Y.; Cai, K.; Yao, Q.; Chen, S.; Chen, L.; He, J. High performance n-type Ag<sub>2</sub>Se film on nylon membrane for flexible thermoelectric power generator. *Nat. Commun.* **2019**, *10*, 841.

(26) Shenasa, M.; Sainkar, S.; Lichtman, D. XPS study of some selected selenium compounds. *J. Electron. Spectros. Relat. Phenomena* **1986**, *40*, 329–337.

(27) Liu, Z. L.; Wu, X.; Shao, Y.; Qi, J.; Cao, Y.; Huang, L.; Liu, C.; Wang, J. O.; Zheng, Q.; Zhu, Z. L.; Ibrahim, K.; Wang, Y. L.; Gao, H. J. Epitaxially grown monolayer VSe<sub>2</sub>: an air-stable magnetic two-dimensional material with low work function at edges. *Sci. Bull.* **2018**, *63*, 419–425.